Optical Materials 31 (2008) 296–299

Contents lists available at ScienceDirect

Optical Materials

journal homepage: www.elsevier.com/locate/optmat

Enhancement of violet and ultraviolet upconversion emissions in Yb^{3+}/Er^{3+}-codoped YF_3 nanocrystals

Guofeng Wang [a], Weiping Qin [a,*], Jisen Zhang [b], Jishuang Zhang [b], Yan Wang [b], Chunyan Cao [b], Lili Wang [a], Guodong Wei [a], Peifen Zhu [a], Ryongjin Kim [a]

[a] State Key Laboratory on Integrated Optoelectronics, College of Electronic Science and Engineering, Jilin University, 2699 Qianjin Street, Changchun 130012, PR China
[b] Key Laboratory of Excited State Processes, Changchun Institute of Optics, Fine Mechanics and Physics, Chinese Academy of Science, Changchun 130033, PR China

ARTICLE INFO

Article history:
Received 28 February 2008
Received in revised form 21 April 2008
Accepted 22 April 2008
Available online 18 June 2008

PACS:
78.66.J
82.80.C

Keywords:
Nanocrystals
Microwave irradiation
Upconversion
Judd–Ofelt parameter

ABSTRACT

Pumped with a 980-nm diode laser, violet/ultraviolet upconversion fluorescence was presented in $Y_{0.83}Yb_{0.15}Er_{0.02}F_3$ nanocrystals. Observed emissions at 318 nm and 379 nm were affirmed coming from a four-photon excitation process. In comparison with a bulk sample having the same chemical compositions, the nanocrystals had a markedly enhanced ability of emitting violet/ultraviolet upconversion fluorescence. By employing Tm^{3+} ions as structural probes in the samples, we found that the enhancement could be attributed to the decrease of Judd–Ofelt parameter Ω_2. A model for revealing the four-photon excitation process was proposed based on spectral analysis.

1. Introduction

Considerable interest has been centered on the frequency upconversion (UC) from infrared (IR) radiation to visible and ultraviolet (UV) by using laser diodes as pump sources and rare-earth (RE) materials as active emissive media [1–5]. Such a research, aimed at developing short-wavelength lasers, is extremely attractive not merely because IR laser diodes are cheap and compact, but also because short-wavelength compact solid-state lasers have potential applications in many fields [6–8]. Since the report of enhanced IR-UV UC of Tm^{3+} ions in fluorides [9], the research on high-order UC has offered a possibility to build UV lasers with RE materials and IR laser diodes. However, why the high-order frequency UC can uniquely happen in some micro- or nano-scaled fluorides still remains a mystery. In previous reports, intense UV UC emissions were mainly observed with Yb^{3+}/Tm^{3+}-codoped fluoride particles and films [10,11], and there four-photon and five-photon processes have been confirmed. However, the high-order (four-photon or five-photon) UC process of Er^{3+} ions is rarely observed due to the rapidly nonradiative energy dissipation of excited Er^{3+} ions and the efficient back energy transfers from excited Er^{3+} ions to neighboring Yb^{3+} ions [5,12].

In this work, we present a four-photon UC process and intense three-photon UC emissions in $Y_{0.83}Yb_{0.15}Er_{0.02}F_3$ nanocrystals under 980-nm excitation. The intensity of 410-nm emission from the nanocrystals is ~44 times stronger than that from a bulk $Y_{0.83}Yb_{0.15}Er_{0.02}F_3$. Even compared to that from the Yb^{3+}/Er^{3+}-codoped YF_3 nanoparticles reported by other researchers [13], the emission peak is also much higher. Judd–Ofelt analysis indicated that the structural parameters of the nanocrystals played key roles in enhancing the violet/UV UC emissions. To explain the four-photon UC process, we proposed an excitation mechanism for the high-order UC in the Yb^{3+}/Er^{3+}-codoped system.

2. Experimental

Hydrofluoric acid (HF), CTAB, cyclohexane, 1-pentanol, and hydrochloric acid (HCl) were supplied by Beijing Chemical Reagent Company, and were of analytical grade. Yttrium oxide (Y_2O_3, 99.99%), ytterbia (Yb_2O_3, 99.99%), and erbium oxide (Er_2O_3, 99.99%) were supplied by Shanghai Chemical Reagent Company. All of the reagents and solvents were used as received without further purification. Distilled water was used to prepare solutions.

* Corresponding author. Tel./fax: +86 431 85168240 8325.
E-mail address: wpqin@jlu.edu.cn (W. Qin).

0925-3467/$ - see front matter © 2008 Elsevier B.V. All rights reserved.
doi:10.1016/j.optmat.2008.04.013

Y_2O_3, Yb_2O_3, and Er_2O_3 were separately dissolved in dilute HCl by heating to prepare the stock solutions of YCl_3, $YbCl_3$, and $ErCl_3$. Two identical solutions, denoted as microemulsion I and II, were prepared by dissolving 2.25 g of CTAB in 50 mL of cyclohexane and 2.5 mL of 1-pentanol. The two microemulsions were stirred separately for 30 min, and then 2 mL of 0.5 M $LnCl_3$ (Ln = Y, Yb, and Er) aqueous solution and 2 mL of 20% HF aqueous solution were added dropwise to microemulsion I and II, respectively. After vigorously stirring, the two optically transparent microemulsion solutions were mixed and stirred for another 10 min and placed in a microwave oven with the power of 700 W for 10 s. The product were then washed thoroughly and dried in vacuum at 80 °C for 24 h. To improve the crystallinity of the nanocrystalline powder, the resultant product was annealed at 450 °C for 2 h in an inert atmosphere. For comparison, the corresponding bulk sample with the same components was prepared by sintering stoichiometric mixture of YF_3 (99.99%), YbF_3 (99.99%), and ErF_3 (99.99%) at 800 °C for 6 h in an inert atmosphere.

Phase identification was performed via X-ray diffractometer (XRD) (modeRigaku RU-200b), using nickel-filtered Cu Kα radiation (λ = 1.5418 Å). The size and morphology of the nanocrystals were characterized by a scanning electron microscope (SEM, KYKY 1000B). Luminescence spectra were recorded with a Hitachi F-4500 fluorescence spectrophotometer.

The XRD patterns of the samples are presented in Fig. 1. All of the diffraction peaks can be readily indexed to those of orthorhombic YF_3 (JCPDS 74-0911). No other impurity peaks are detected. Taking account of the effect of instrumental broadening, the average crystalline size of nanocrystals was estimated to be about 80 nm by the Scherrer equation. The observation of SEM (Fig. 2) indicated that the nanocrystals tended to aggregate.

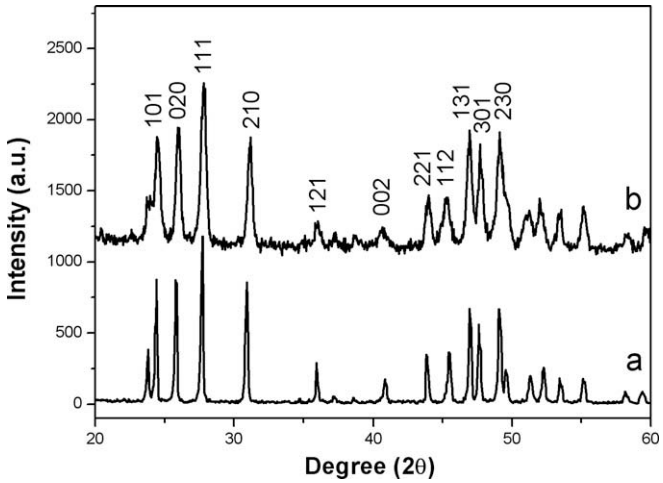

Fig. 1. XRD patterns of $Y_{0.83}Yb_{0.15}Er_{0.02}F_3$: (a) bulk sample; (b) nanocrystals.

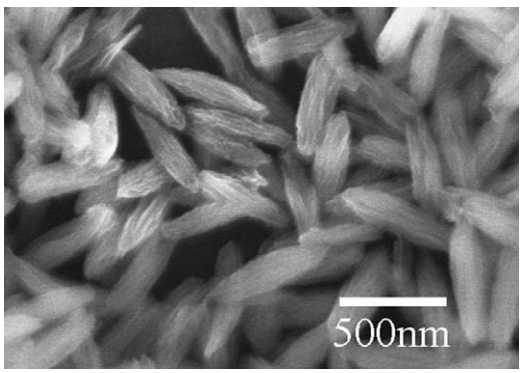

Fig. 2. SEM image of $Y_{0.83}Yb_{0.15}Er_{0.02}F_3$ nanocrystals.

3. Results and discussion

When the 980-nm diode laser with a 220-mW output was focused on the nanocrystals, strong UC fluorescence was visible to the naked eye in daylight. Under the near IR excitation (~260 W/cm^2), UC spectra of the nanosized and bulk samples were recorded at room temperature, as shown in Fig. 3. The spectral peaks correspond to the following transitions: $^2P_{3/2} \rightarrow {}^4I_{15/2}$ (~318 nm), $^4G_{11/2} \rightarrow {}^4I_{15/2}$ (~379 nm), $^2H_{9/2} \rightarrow {}^4I_{15/2}$ (~410 nm), $^2P_{3/2} \rightarrow {}^4I_{11/2}$ (~470 nm), $^2H_{11/2} \rightarrow {}^4I_{15/2}$ (~522 nm), $^4S_{3/2} \rightarrow {}^4I_{15/2}$ (~545 nm), and $^4F_{9/2} \rightarrow {}^4I_{15/2}$ (~652 nm). In comparison with those of the bulk sample, violet and UV emissions from the nanocrystals are greatly enhanced. The luminescence intensity at 410 nm is ~3 times stronger than that at 652 nm for the nanocrystals, while the 652-nm emission is dominant in the bulk sample and the luminescence intensity at 410 nm is less than 7% of it. Here, we used a PMT (Hamamatsu R928) as the detector, and therefore the relative intensity ratio of the two emissions reflects the relative ratio of them in photons/second.

The radiative transition $^2P_{3/2} \rightarrow {}^4I_{15/2}$ of Er^{3+} ions has never been observed under 980-nm excitation before this work. The 318-nm emission came from this transition, and, under 980-nm excitation, it should be a four-photon excitation process. To prove the correctness of the judgment, we have checked the power dependence of the UC luminescence intensity. For an unsaturated UC, the emission intensity is proportional to the nth power of the excitation intensity, and the integer n is the number of photons absorbed per upconverted photon emitted [14]. Fig. 4 shows the power dependence of the UC emission intensities: n = 3.855, 3.133, and 2.932 for 318-, 379-, and 410-nm emissions, respectively. The proposed processes of IR excitation and UC emission were drawn in the energy level diagrams of Er^{3+} and Yb^{3+} ions, as shown in Fig. 5. There were two processes serving for populating the state $^2H_{9/2}$ and 410-nm emission: (1) $^2F_{5/2}$ (Yb) + $^4F_{9/2}$ (Er) → $^2F_{7/2}$ (Yb) + $^2H_{9/2}$ (Er); and (2) $^2F_{5/2}$ (Yb) + $^4S_{3/2}$ (Er) → $^2F_{7/2}$ (Yb) + $^2G_{7/2}$ (Er), followed by fast cascading relaxation from the $^2G_{7/2}$ to the $^2H_{9/2}$ state [6]. Subsequent nonradiative relaxation from the $^2G_{7/2}$ to the $^4G_{11/2}$ also populated the $^4G_{11/2}$ level, which conduced to 379-nm emission. It is imperative to point out that another four-

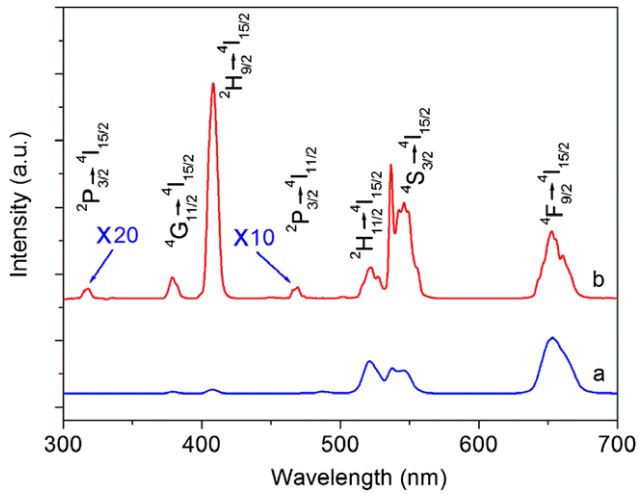

Fig. 3. UC emission spectra of $Y_{0.83}Yb_{0.15}Er_{0.02}F_3$ under 980-nm excitation: (a) bulk sample; (b) nanocrystals.

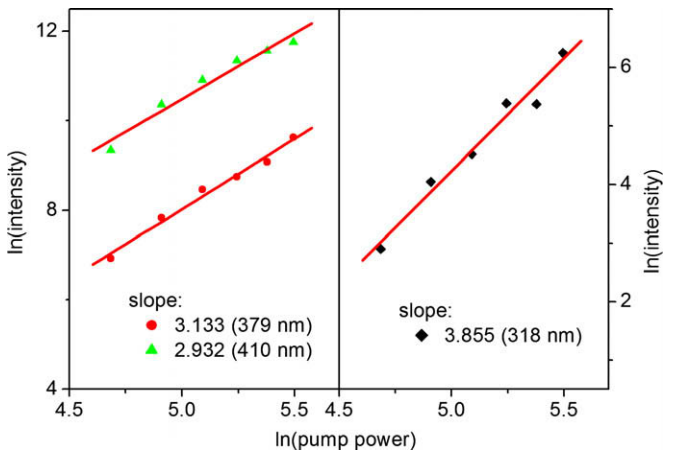

Fig. 4. Ln–ln plot of the UC fluorescence intensity versus the pump power at 318 nm (♦), 379 nm (●), and 410 nm (▲) in $Y_{0.83}Yb_{0.15}Er_{0.02}F_3$ nanocrystals.

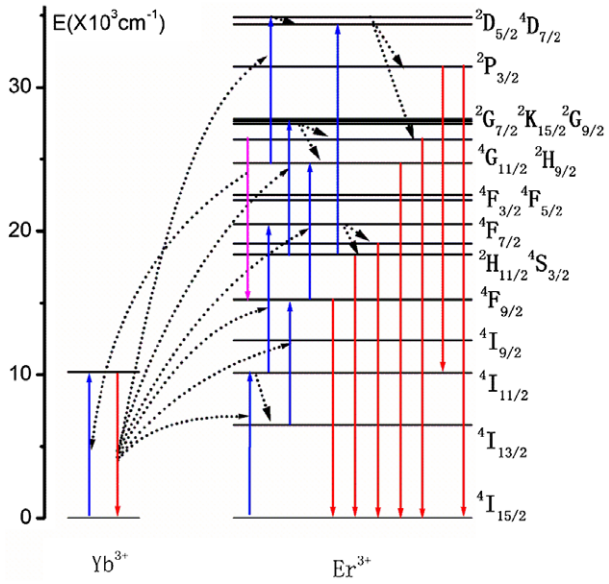

Fig. 5. UC mechanism of Yb^{3+}-sensitized Er^{3+} emissions in YF_3 nanocrystals.

photon process, $^4D_{7/2} \rightarrow {}^4G_{11/2}$, was involved in populating the $^4G_{11/2}$ level. Two possible mechanisms might be responsible for populating the $^4D_{7/2}$ level: (1) co-sensitizing effect: $2\,^2F_{5/2}$ (Yb) + $^4F_{9/2}$ (Er) → $2\,^2F_{7/2}$ (Yb) + $^4D_{7/2}$ (Er); and (2) energy transfer: $^2F_{2/5}$ (Yb) + $^2H_{9/2}$ (Er) → $^2F_{7/2}$ (Yb) + $^2D_{5/2}$ (Er), followed by a nonradiative decay to the $^4D_{7/2}$ state [15]. For 318/470-nm emission, the $^2P_{3/2}$ level was populated by a (radiative or nonradiative) transition from the $^2D_{5/2}/^4D_{7/2}$ state. Taking the $^2P_{3/2} \rightarrow {}^4S_{3/2}$ transition [16] into account, the increased population of the $^2P_{3/2}$ level induced the enhancement of the $^4S_{3/2} \rightarrow {}^4I_{15/2}$ emission.

Our previous results indicated that UC luminescence intensities were not only determined by the excitation power density but also strongly dependent on the concentration of dopant and the surrounding of activators in samples [2,10,11]. To study the effect of dopant concentrations on the violet/UV UC emissions, the dependence of Er^{3+} and Yb^{3+} concentrations on the fluorescence was studied, for both nanosized and bulk samples. The results indicated that strong violet/UV UC fluorescence from nanocrystals could be easily observed, but whatever concentrations of Yb^{3+} and Er^{3+} were adjusted, it could not be observed for bulk samples. Therefore, the enhancement of violet/UV UC in nanocrystals was not caused by the change of dopant concentrations. Presumably, three mechanisms might cause the enhancement of violet/UV UC in the nanocrystals. (1) The excitation light was trapped inside nanoparticles due to their small sizes and relative large surface/volume ratio [9], so the actual excitation power density inside was much higher than that in a bulk sample. However, it is difficult to check the effect of light trapping experimentally under current experimental condition. (2) In comparison with that of the bulk sample, the faster nonradiative relaxation of $^2H_{11/2}$ to $^4S_{3/2}$ results in efficient population of $^4S_{3/2}$ level in nanocrystals [17], which is benefit for the energy transfer of $^2F_{5/2}$ (Yb) + $^4S_{3/2}$ (Er) → $^2F_{7/2}$ (Yb) + $^2G_{7/2}$ (Er). Similarly, the faster nonradiative relaxation of $^2G_{7/2}/^4G_{11/2}$ to $^2H_{9/2}$ leads to the enhancement of $^2H_{9/2} \rightarrow {}^4I_{15/2}$ transition in nanocrystals. (3) The surrounding of Er^{3+} ions in the nanocrystals was more benefit for violet/UV UC emissions. Our group and Chen's group have attributed the violet/UV enhancement to the decrease of Judd–Ofelt (J–O) parameter Ω_2 [1,2,11], which reflects the symmetry of the crystal field. In order to clarify the structural difference between the nanocrystals and the bulk material, we doped thulium in both samples instead of erbium and employed Tm^{3+} ions as structural probes to explore their surroundings. Tm^{3+} is an excellent activator for frequency UC, and additionally its spectrum changes sensitively with surroundings. According to Ref. [1], the local structural variation and how the variation results in the change of spectral properties in different samples can be verified by following J–O analysis.

With the help of J–O parameters Ω_λ ($\lambda = 2, 4, 6$), the radiative transition probability between states J and J' can be expressed as

$$A_{JJ'} = \frac{64\pi^4 e^2}{3hc^2}\frac{\nu^3}{2J+1}\frac{n(n^2+2)^2}{9}\sum_{\lambda=2,4,6}\Omega_\lambda \langle \Psi' J' || U^{(\lambda)} || \Psi J \rangle^2 \quad (1)$$

here, e, c, n, h, ν, and $\langle \Psi' J' || U^{(\lambda)} || \Psi J \rangle^2$ represent elementary charge, velocity of light in vacuum, refractive index, Planck constant, mean wavenumber, and doubly reduced matrix elements, respectively. Since the doubly reduced matrix element $\langle || U^{(2)} || \rangle^2$ of the $^1D_2 \rightarrow {}^3F_4$ transition (452 nm) of Tm^{3+} ions is large, the branching ratio (β_{452}) of 452-nm emission would be largely enhanced by increasing Ω_2 [2]. In addition, β_{452} approximates the intensity ratio $R = I_{452}/(I_{362} + I_{452})$ due to $\beta_{452} + \beta_{362} \approx 1$, where β_{362} is the branching ratio of the $^1D_2 \rightarrow {}^3H_6$ transition (362 nm), so an changed intensity ratio R can reflect the change of Ω_2 [11]. From the UC emission spectra of Yb^{3+}/Tm^{3+} codoped YF_3 samples (Fig. 6), we calculated $R = 0.40$ for the nanocrystals and $R = 0.64$ for the bulk sample. This

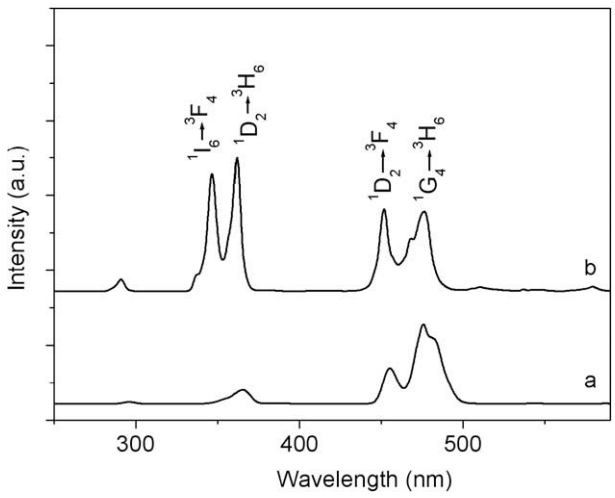

Fig. 6. UC emission spectra of $Y_{0.83}Yb_{0.15}Tm_{0.02}F_3$ under 980-nm excitation: (a) bulk sample; (b) nanocrystals.

Table 1
Doubly reduced matrix elements of the $^4G_{11/2} \rightarrow {}^4F_{9/2}$ transition of Er^{3+}

Transition	$(U^{(2)})^2$	$(U^{(4)})^2$	$(U^{(6)})^2$
$^4G_{11/2} \rightarrow {}^4F_{9/2}$ (Er^{3+})	0.4283	0.0372	0.0112

change of R in different samples means that Ω_2 in the nanocrystals is smaller than that in the bulk sample.

For the Yb^{3+}/Er^{3+} codoped nanocrystals, enhanced violet/UV emissions and faded 652-nm emission came from the similar reason, a decreased Ω_2, which resulted in the reduced $^4G_{11/2} \rightarrow {}^4F_{9/2}$ transition [2]. Considering Eq. (1) and the doubly reduced matrix elements of the $^4G_{11/2} \rightarrow {}^4F_{9/2}$ transition of Er^{3+} ions, as listed in Table 1 [18], the transition rate from the $^4G_{11/2}$ to the $^4F_{9/2}$ will decrease dramatically with the decrease of Ω_2, and therefore the transition of $^4G_{11/2} \rightarrow {}^4I_{15/2}$ will become stronger. Subsequently enhanced nonradiative relaxation from the $^4G_{11/2}$ to the $^2H_{9/2}$ also resulted in efficient population of the state $^2H_{9/2}$, which make the state $^2D_{5/2}$ populated efficiently by the energy transfer of $^2F_{2/5}$ (Yb) + $^2H_{9/2}$ (Er) $\rightarrow {}^2F_{7/2}$ (Yb) + $^2D_{5/2}$ (Er) and also increase the population of the $^2P_{3/2}$ by nonradiative relaxation of $^2D_{5/2} \rightarrow {}^2P_{3/2}$. Consequently, intense violet/UV luminescence was obtained in $Y_{0.83}Yb_{0.15}Er_{0.02}F_3$ nanocrystals.

4. Conclusions

In summary, we presented a four-photon UC process of Er^{3+} ions in $Y_{0.83}Yb_{0.15}Er_{0.02}F_3$ nanocrystals pumped with a 980-nm diode laser. In comparison with the bulk sample, the nanoparticles can emit enhanced violet and UV UC fluorescence. By employing Tm^{3+} as a structure probe, we found that the structural parameter Ω_2 in the nanocrystals was smaller than that in the bulk material. The reduced Ω_2 has induced an increase of the population in the $^4G_{11/2}$ (Er) and the enhanced violet and UV emissions in the nanocrystals.

Acknowledgement

This work was supported by the National Natural Science Foundation of China (Grant Nos. 10474096 and 50672030).

References

[1] D. Chen, Y. Wang, Y. Yu, P. Huang, Appl. Phys. Lett. 91 (2007) 051920.
[2] G. Qin, W. Qin, S. Huang, C. Wu, D. Zhao, B. Chen, S. Lu, J. Appl. Phys. 92 (2002) 6936.
[3] M. Daisuke, Appl. Phys. Lett. 81 (2002) 4526.
[4] B. Dong, D. Liu, X. Wang, T. Yang, S. Miao, C. Li, Appl. Phys. Lett. 90 (2007) 181117.
[5] Y. Wang, J. Ohwaki, Appl. Phys. Lett. 63 (1993) 3268.
[6] T. Hebert, R. Wannemacher, W. Lenth, R.M. Macfarlane, Appl. Phys. Lett. 57 (1990) 1727.
[7] Y. Mita, K. Hirama, N. Ando, H. Yamamoto, S. Shionoya, J. Appl. Phys. 74 (1993) 4703.
[8] E. Downing, L. Hesselink, J. Ralston, R. Macfarlane, Science 273 (1996) 1185.
[9] W. Qin, G. Qin, J. Korean Phys. Soc. 44 (2004) 925.
[10] G. De, W. Qin, J. Zhang, J. Zhang, Y. Wang, C. Cao, Y. Cui, J. Lumin. 122–123 (2007) 128.
[11] G. Qin, W. Qin, C. Wu, S. Huang, J. Zhang, S. Lu, D. Zhao, H. Liu, J. Appl. Phys. 93 (2003) 4328.
[12] F. Vetrone, J.C. Boyer, J.A. Capobianco, J. Appl. Phys. 96 (2004) 661.
[13] R. Yan, Y. Li, Adv. Funct. Mater. 15 (2005) 763.
[14] M. Pollnau, D.R. Gamelin, S.R. Lüthi, H.U. Güdel, Phys. Rev. B 61 (2000) 3337.
[15] X. Mateos, R. Solé, J. Gavaldà, M. Aguiló, F. Díaz, J. Massons, J. Lumin. 115 (2005) 131.
[16] G. Chen, Y. Liu, Z. Zhang, B. Aghahadi, G. Somesfalean, Q. Sun, F. Wang, Chem. Phys. Lett. 448 (2007) 127.
[17] X. Bai, H. Song, G. Pan, Y. Lei, T. Wang, X. Ren, S. Lu, B. Dong, Q. Dai, L. Fan, J. Phys. Chem. C 111 (2007) 13611.
[18] R.C. Pappalarto, J. Lumin. 14 (1976) 159.